Asociación Argentina
de Mecánica Computacional

Mecánica Computacional Vol XXV, pp. 1861-1878
Alberto Cardona, Norberto Nigro, Victorio Sonzogni, Mario Storti. (Eds.)
Santa Fe, Argentina, Noviembre 2006

ELASTO-PLASTIC ANALYSIS OF STRUCTURES USING HEXAHEDRICAL ELEMENTS WITH EIGHT NODES AND ONE-POINT QUADRATURE

Dilnei Schmidt[a], Armando M. Awruch[b] and Inácio B. Morsh[b]

[a]*Centro de Mecânica Aplicada e Computacional (CEMACOM), Universidade Federal do Rio Grande do Sul, Av. Osvaldo Aranha, 99, 3º andar, 90035-190, Porto Alegre, RS, Brasil, dilnei_s@hotmail.com, http://www.cpgec.ufrgs.br*
[b]*Centro de Mecânica Aplicada e Computacional (CEMACOM), Universidade Federal do Rio Grande do Sul, Av. Osvaldo Aranha, 99, 3º andar, 90035-190, Porto Alegre, RS, Brasil, amawruch@ufrgs.br, http://www.cpgec.ufrgs.br*

Keywords: Elasto-plastic analysis, Geometrically nonlinear analysis, Hexahedrical element with one-point quadrature

Abstract. The main purposes of this work are the formulation and application of a computational algorithm for the elasto-plastic static analysis of structures, including finite displacements and rotations. An hexahedrical isoparametric finite element with eight nodes and one-point quadrature is used. Mechanisms to avoid hourglass modes as well as volumetric and shear locking are introduced. A corotational formulation is employed to deal with the geometrically nonlinear analysis, whereas an explicit algorithm (based in Euler's scheme) is implemented for the elasto-plastic analysis. The applied constitutive models include the Mohr-Coulomb as well as the Von Mises yield criterion with isotropic hardening. Numerical examples with highly nonlinear behavior are presented to demonstrate the range of applicability of the formulation.

1 INTRODUCTION

Low order three-dimensional finite elements have been used with efficiency in many solid mechanics problems. However, volumetric locking is encountered for incompressible or near incompressible materials and shear locking appears in bending-dominated situations when no special element technology is embedded to overcome this deficiency. Among the ideas to eliminate this problem, reduced integration may be used. Nevertheless, the results achieved through the use of these elements can be unsatisfactory or even meaningless when spurious modes are excited. Hence, the use of the reduced integration elements requires an efficient numerical stabilization scheme to suppress the spurious modes.

Low order finite elements with reduced integration and hourglass stabilization are especially attractive due to their computational efficiency. The numerical efficiency gained by working with a lower number of Gauss points is in particular noticeable when the numerical cost of a finite element analysis is strongly coupled to the numerical effort at the element level. This is the case when explicit computations are performed and also computations based on highly complex constitutive models.

In a non-linear finite element analysis, it is necessary to integrate the constitutive relations to obtain the unknown increment in the stresses. These relations define a set of ordinary differential equations and methods for integrating them are usually classified as explicit or implicit. Since explicit schemes employ the standard elasto-plastic constitutive law and require only first derivatives of the yield function and plastic potential, they can be used to design a general purpose integrator, as the one proposed by Sloan *et al*. (2001), which can be used for a wide range of models. By being more straightforward to implement than implicit methods, an explicit method will be used in this work to integrate the constitutive relations.

Several authors have been working in the subject of low order finite elements with hourglass stabilization. The three-dimensional reduced integration concept was mainly developed by Belytschko, Liu and coworkers. Liu *et al*. (1994) developed an underintegrated eight-node hexahedral element where the dilatational term of the normal strain components as well as some shear strain components are treated in a special way. Based on the multiple-quadrature formulation given in Liu *et al*. (1994), Hu and Nagy (1997) as well as Duarte Filho and Awruch (2004) proposed a new simple one-point quadrature hexahedral element. The strain and stress vectors are firstly expanded in a Taylor series at the element center up to bilinear terms. The constant terms are used to compute the element internal force vector and the linear and bilinear terms are used to form the hourglass resisting force vector. As shown in Liu *et al*. (1994), the corotational system is employed to remove those modes associated with shear locking and the dilatational part of the gradient matrix is evaluated only at the center of the element to avoid volumetric locking.

In the formulation of Liu *et al*. (1998), the element proposed by Liu *et al*. (1994) is implemented for large deformation elasto-plastic analysis. The authors work with four point quadrature which has the advantage that plastic front can be captured more accurately. On the other hand, the advantage of computational efficiency is partially lost.

Thus, the objective of this work is to verify the computational efficiency and the robustness of the eight-node hexahedral element with one-point quadrature developed by Hu and Nagy (1997) and by Duarte Filho and Awruch (2004), added with the elasto-plastic scheme proposed by Sloan *et al.* (2001), in the analysis of structural and geotechnical problems. The numerical simulation presented here was compared with results obtained by others authors and by a commercial software and it is shown that critical problems with physical and geometrically nonlinear analysis may be solved with the one-point quadrature three-dimensional element.

2 PRINCIPLE OF VIRTUAL WORK

In a finite element representation, the principle of virtual work is given by:

$$\delta \mathbf{W}_e^{\text{int}} = \int_{V_e} \delta \mathbf{u}^t \mathbf{b} \ \ \mathrm{d}V + \int_{S_e} \delta \mathbf{u}^t \bar{\mathbf{p}} \ \ \mathrm{d}S \,, \tag{1}$$

where the superscript t designates the transpose; $\delta\mathbf{u}$ is the virtual displacement vector in the element "e"; $\mathbf{b}$ is the body force vector applied in the element domain V_e; $\bar{\mathbf{p}}$ is the traction vector applied on the element boundary S_e; $\mathbf{W}_e^{\text{int}}$ is the element internal virtual work given by:

$$\delta \mathbf{W}_e^{\text{int}} = \int_{V_e} \delta \boldsymbol{\varepsilon}^t \boldsymbol{\sigma} \ \ \mathrm{dV} \,, \tag{2}$$

where $\boldsymbol{\sigma}$ is the stress vector in the element and $\delta\varepsilon$ is the virtual strain vector due to $\delta\mathbf{u}$.

If the strain in the element is interpolated in terms of nodal displacement by:

$$\boldsymbol{\varepsilon} = \bar{\mathbf{B}} \ \ \mathbf{U}^e \,, \tag{3}$$

then, equation 2 can be rewritten as:

$$\delta \mathbf{W}_e^{\text{int}} = \delta \mathbf{U}^{e\,t} \int_{V_e} \bar{\mathbf{B}}^t \boldsymbol{\sigma} \ \ \mathrm{d}V \,, \tag{4}$$

where $\bar{\mathbf{B}}$ is the gradient matrix.

3 ONE-POINT QUADRATURE EIGHT-NODE HEXAHEDRAL ELEMENT WITH HOURGLASS CONTROL

For an eight-node hexahedral element, the spatial coordinates, x_i, and the displacement components, u_i, in the element are approximated in terms of nodal values, x_{ia} and u_{ia}, by:

$$x_i = \sum_{a=1}^{8} N_a x_{ia} \,, \tag{5}$$

$$u_i = \sum_{a=1}^{8} N_a u_{ia} \,, \tag{6}$$

where the trilinear shape functions are expressed as:

$$N_a(\xi,\eta,\zeta) = \frac{1}{8}(1+\xi_a\xi)(1+\eta_a\eta)(1+\zeta_a\zeta) \,, \tag{7}$$

and the subscript i denotes coordinate components (x, y, z) ranging from one to three and a denotes the element nodal numbers ranging from one to eight. The referential coordinates ξ, η e ζ of node a are denoted by ξ_a, η_a e ζ_a, respectively.

If the following column vectors are defined for nodal coordinates in the spatial system and the natural system:

$$\mathbf{x}_1^t = \mathbf{x}^t = \left[x_1, x_2, x_3, x_4, x_5, x_6, x_7, x_8\right], \tag{8}$$

$$\mathbf{x}_2^t = \mathbf{y}^t = \left[y_1, y_2, y_3, y_4, y_5, y_6, y_7, y_8\right], \tag{9}$$

$$\mathbf{x}_3^t = \mathbf{z}^t = \left[z_1, z_2, z_3, z_4, z_5, z_6, z_7, z_8\right], \tag{10}$$

$$\boldsymbol{\xi}^t = \left[-1,+1,+1,-1,-1,+1,+1,-1\right], \tag{11}$$

$$\boldsymbol{\eta}^t = \left[-1,-1,+1,+1,-1,-1,+1,+1\right], \tag{12}$$

$$\boldsymbol{\zeta}^t = \left[-1,-1,-1,-1,+1,+1,+1,+1\right], \tag{13}$$

the Jacobian matrix at the center of the element ($\xi = \eta = \zeta = 0$) can be evaluated as:

$$\mathbf{J}(\mathbf{0}) = \frac{1}{8}\begin{bmatrix} \boldsymbol{\xi}^t\mathbf{x} & \boldsymbol{\xi}^t\mathbf{y} & \boldsymbol{\xi}^t\mathbf{z} \\ \boldsymbol{\eta}^t\mathbf{x} & \boldsymbol{\eta}^t\mathbf{y} & \boldsymbol{\eta}^t\mathbf{z} \\ \boldsymbol{\zeta}^t\mathbf{x} & \boldsymbol{\zeta}^t\mathbf{y} & \boldsymbol{\zeta}^t\mathbf{z} \end{bmatrix}, \tag{14}$$

and its determinant j_o can be written as:

$$j_o = \det\left|\mathbf{J}(\mathbf{0})\right| = \frac{1}{512}\begin{vmatrix} \boldsymbol{\xi}^t\mathbf{x} & \boldsymbol{\xi}^t\mathbf{y} & \boldsymbol{\xi}^t\mathbf{z} \\ \boldsymbol{\eta}^t\mathbf{x} & \boldsymbol{\eta}^t\mathbf{y} & \boldsymbol{\eta}^t\mathbf{z} \\ \boldsymbol{\zeta}^t\mathbf{x} & \boldsymbol{\zeta}^t\mathbf{y} & \boldsymbol{\zeta}^t\mathbf{z} \end{vmatrix} = \frac{1}{8}V_e, \tag{15}$$

where V_e is the volume of the 8-node hexahedral element.

To identify the deformation modes of the element, as it can be seen in Liu *et al*. (1994), the gradient submatrices $\mathbf{B}_a(\mathbf{0})$ at the center of the element are defined as follows:

$$\mathbf{B}_a(\mathbf{0}) = \begin{bmatrix} \dfrac{\partial \mathbf{N}_a(0)}{\partial x} \\ \dfrac{\partial \mathbf{N}_a(0)}{\partial y} \\ \dfrac{\partial \mathbf{N}_a(0)}{\partial z} \end{bmatrix} = \begin{bmatrix} \mathbf{b}_1 \\ \mathbf{b}_2 \\ \mathbf{b}_3 \end{bmatrix}, \ (\text{a} = 1,2,...,8). \tag{16}$$

If the inverse matrix of $\mathbf{J(0)}$ is denoted by $\mathbf{D}$, then the gradient vectors $\mathbf{b}_1$, $\mathbf{b}_2$ and $\mathbf{b}_3$ in equation 16, according to Liu *et al*. (1998), can be shown to be:

$$\mathbf{b}_1 = \{b_{1a}\} = \frac{1}{8}\left[D_{11}\boldsymbol{\xi} + D_{12}\boldsymbol{\eta} + D_{13}\boldsymbol{\zeta}\ \right], \tag{17}$$

$$\mathbf{b}_2 = \{b_{2a}\} = \frac{1}{8}\left[D_{21}\boldsymbol{\xi} + D_{22}\boldsymbol{\eta} + D_{23}\boldsymbol{\zeta}\ \right], \tag{18}$$

$$\mathbf{b}_3 = \{b_{3a}\} = \frac{1}{8}\left[D_{31}\boldsymbol{\xi} + D_{32}\boldsymbol{\eta} + D_{33}\boldsymbol{\zeta}\ \right]. \tag{19}$$

To alleviate volumetric locking, the idea underlying reduced-selective integration is used. The gradient matrix is decomposed into two parts:

$$\bar{\mathbf{B}}(\xi,\eta,\zeta) = \tilde{\mathbf{B}}(\mathbf{0}) + \hat{\mathbf{B}}(\xi,\eta,\zeta), \tag{20}$$

where $\tilde{\mathbf{B}}(\mathbf{0})$ is the gradient matrix corresponding to the dilatational part of the strain vector, evaluated at the element center only, and $\hat{\mathbf{B}}(\xi,\eta,\zeta)$ is the gradient matrix corresponding to the deviatoric part of the strain vector.
Then, equation 4 can be rewritten as:

$$\delta \mathbf{W}_e^{\text{int}} = \delta \mathbf{U}^{e\ t} \int_{V_e} [\ \tilde{\mathbf{B}}^t(\mathbf{0}) + \hat{\mathbf{B}}^t(\xi,\eta,\zeta)\ ]\ \boldsymbol{\sigma}(\xi,\eta,\zeta)\ dV\,. \tag{21}$$

Expanding $\hat{\mathbf{B}}(\xi,\eta,\zeta)$ in a Taylor series at the element center up to bilinear terms, equation 20 can be rewritten as:

$$\begin{aligned}\bar{\mathbf{B}}(\xi,\eta,\zeta) = \mathbf{B}(\mathbf{0}) + \hat{\mathbf{B}}_{,\xi}(\mathbf{0})\xi + \hat{\mathbf{B}}_{,\eta}(\mathbf{0})\eta + \hat{\mathbf{B}}_{,\zeta}(\mathbf{0})\zeta + \\ 2\hat{\mathbf{B}}_{,\xi\eta}(\mathbf{0})\xi\eta + 2\hat{\mathbf{B}}_{,\eta\zeta}(\mathbf{0})\eta\zeta + 2\hat{\mathbf{B}}_{,\xi\zeta}(\mathbf{0})\xi\zeta\,,\end{aligned} \tag{22}$$

where **B(0)** is the one-point quadrature gradient matrix contributed from both the dilatational and deviatoric parts:

$$\mathbf{B}(\mathbf{0}) = \tilde{\mathbf{B}}(\mathbf{0}) + \hat{\mathbf{B}}(\mathbf{0})\,. \tag{23}$$

The other terms on the right-hand side of equation 22 are the gradient matrices corresponding to non-constant deviatoric strain. The first and second derivatives of $\bar{\mathbf{B}}$ are obtained after some tedious algebra and can be found in Liu *et al*. (1998).

The stress vector is also expanded in a Taylor series about the element center up to bilinear terms:

$$\begin{aligned}\boldsymbol{\sigma}(\xi,\eta,\zeta) = \boldsymbol{\sigma}(\mathbf{0}) + \hat{\boldsymbol{\sigma}}_{,\xi}(\mathbf{0})\xi + \hat{\boldsymbol{\sigma}}_{,\eta}(\mathbf{0})\eta + \hat{\boldsymbol{\sigma}}_{,\zeta}(\mathbf{0})\zeta + \\ 2\hat{\boldsymbol{\sigma}}_{,\xi\eta}(\mathbf{0})\xi\eta + 2\hat{\boldsymbol{\sigma}}_{,\eta\zeta}(\mathbf{0})\eta\zeta + 2\hat{\boldsymbol{\sigma}}_{,\xi\zeta}(\mathbf{0})\xi\zeta\,.\end{aligned} \tag{24}$$

By substituting equation 22 and equation 24 into equation 21, we can integrate and obtain the internal virtual work of the element as:

$$\begin{aligned}\delta \mathbf{W}_e^{\text{int}} = \delta \mathbf{U}^{e\ t} \Big[\ \mathbf{B}^t(\mathbf{0})\boldsymbol{\sigma}(\mathbf{0}) + \frac{1}{3}\hat{\mathbf{B}}^t_{,\xi}(\mathbf{0})\hat{\boldsymbol{\sigma}}_{,\xi}(\mathbf{0}) + \frac{1}{3}\hat{\mathbf{B}}^t_{,\eta}(\mathbf{0})\hat{\boldsymbol{\sigma}}_{,\eta}(\mathbf{0}) + \frac{1}{3}\hat{\mathbf{B}}^t_{,\zeta}(\mathbf{0})\hat{\boldsymbol{\sigma}}_{,\zeta}(\mathbf{0}) + \\ \frac{1}{9}\hat{\mathbf{B}}^t_{,\xi\eta}(\mathbf{0})\hat{\boldsymbol{\sigma}}_{,\xi\eta}(\mathbf{0}) + \frac{1}{9}\hat{\mathbf{B}}^t_{,\eta\zeta}(\mathbf{0})\hat{\boldsymbol{\sigma}}_{,\eta\zeta}(\mathbf{0}) + \frac{1}{9}\hat{\mathbf{B}}^t_{,\xi\zeta}(\mathbf{0})\hat{\boldsymbol{\sigma}}_{,\xi\zeta}(\mathbf{0})\ \Big] V_e\,,\end{aligned} \tag{25}$$

where the first term on the right-hand side of equation 25 is the one-point quadrature internal virtual work. The other terms are also evaluated at the element center to provide the stabilization of the element.

By assuming that the Jacobian is a constant, 1/8 of the element volume, the one-point quadrature element internal force vector without hourglass control can be expressed by:

$$\mathbf{f}^e = \mathbf{B}^t(\mathbf{0})\ \boldsymbol{\sigma}(\mathbf{0})\ V_e\,. \tag{26}$$

The element stiffness matrix for the underintegrated element can be obtained by using the stress-strain law $\boldsymbol{\sigma} = \mathbf{C}\boldsymbol{\varepsilon}$ in conjunction with the strain displacement relation given by equation 3:

$$\mathbf{f}^e = \mathbf{K}^e\ \ \mathbf{U}^e\,, \tag{27}$$

where $\mathbf{K}^e$ is the element stiffness matrix evaluated at the element center without hourglass control and it is given by:

$$\mathbf{K}^e = \mathbf{B}^t(\mathbf{0})\ \mathbf{C}\ \mathbf{B}(\mathbf{0})\ V_e\,, \tag{28}$$

which is rank insufficient and may exhibit spurious singular modes. To eliminate these spurious singular modes, it is necessary to add the hourglass-resisting force, $\mathbf{f}^{hg}$, to the element internal force vector as:

$$\mathbf{f}^{\text{int}} = \mathbf{f}^{e} + \mathbf{f}^{hg} . \tag{29}$$

By observing equation 25, 26 and 29, $\mathbf{f}^{hg}$ may be defined as:

$$\begin{aligned} \mathbf{f}^{hg} = \Bigg[& \frac{1}{3}\hat{\mathbf{B}}^{t}_{,\xi}(\mathbf{0})\,\hat{\boldsymbol{\sigma}}_{,\xi}(\mathbf{0}) + \frac{1}{3}\hat{\mathbf{B}}^{t}_{,\eta}(\mathbf{0})\,\hat{\boldsymbol{\sigma}}_{,\eta}(\mathbf{0}) + \frac{1}{3}\hat{\mathbf{B}}^{t}_{,\zeta}(\mathbf{0})\,\hat{\boldsymbol{\sigma}}_{,\zeta}(\mathbf{0}) + \\ & \frac{1}{9}\hat{\mathbf{B}}^{t}_{,\xi\eta}(\mathbf{0})\,\hat{\boldsymbol{\sigma}}_{,\xi\eta}(\mathbf{0}) + \frac{1}{9}\hat{\mathbf{B}}^{t}_{,\eta\zeta}(\mathbf{0})\,\hat{\boldsymbol{\sigma}}_{,\eta\zeta}(\mathbf{0}) + \frac{1}{9}\hat{\mathbf{B}}^{t}_{,\xi\zeta}(\mathbf{0})\,\hat{\boldsymbol{\sigma}}_{,\xi\zeta}(\mathbf{0}) \Bigg] V_e . \end{aligned} \tag{30}$$

If the first and second derivatives of the stress vector can be derived from the material constitutive equations, the element stabilization stiffness matrix $\mathbf{K}^{stab}$ may be also defined as:

$$\mathbf{f}^{hg} = \mathbf{K}^{stab} \quad \mathbf{U}^{e} . \tag{31}$$

This matrix is added to the element stiffness matrix, $\mathbf{K}^{e}$, so the element stiffness matrix $\mathbf{K}$ is rank sufficient and is given by:

$$\mathbf{K} = \mathbf{K}^{e} + \mathbf{K}^{stab} . \tag{32}$$

To avoid the derivation of the relationships between the first and second derivative of the stress vector and the nodal displacement vector in equation 30, Hu and Nagy (1997) proposed a "stabilization matrix", $\mathbf{E}$, to satisfy following constitutive relations:

$$\begin{aligned} & \hat{\boldsymbol{\sigma}}_{,\xi} = \mathbf{E}\ \hat{\boldsymbol{\varepsilon}}_{,\xi} , \quad \hat{\boldsymbol{\sigma}}_{,\eta} = \mathbf{E}\ \hat{\boldsymbol{\varepsilon}}_{,\eta} , \quad \hat{\boldsymbol{\sigma}}_{,\zeta} = \mathbf{E}\ \hat{\boldsymbol{\varepsilon}}_{,\zeta} , \\ & \hat{\boldsymbol{\sigma}}_{,\xi\eta} = \mathbf{E}\ \hat{\boldsymbol{\varepsilon}}_{,\xi\eta} , \quad \hat{\boldsymbol{\sigma}}_{,\eta\zeta} = \mathbf{E}\ \hat{\boldsymbol{\varepsilon}}_{,\eta\zeta} , \quad \hat{\boldsymbol{\sigma}}_{,\xi\zeta} = \mathbf{E}\ \hat{\boldsymbol{\varepsilon}}_{,\xi\zeta} . \end{aligned} \tag{33}$$

where $\mathbf{E}$ is the elastic material modulus matrix, which is the simplest form for computation and is given as:

$$\mathbf{E}_{6x6} = \begin{bmatrix} \mathbf{e}_{3x3} & \mathbf{0} \\ \mathbf{0} & \mathbf{e}_{3x3} \end{bmatrix}, \tag{34}$$

where,

$$\mathbf{e} = \begin{bmatrix} 2\mu & 0 & 0 \\ 0 & 2\mu & 0 \\ 0 & 0 & 2\mu \end{bmatrix}, \tag{35}$$

and μ is the Lamé constant.

Elasto-plastic material behavior or damage is characterized by a sudden softening of the material if a certain stress limit is reached. To prevent excessive stiffness and enhance the behavior of elasto-plastic materials, Reese (2005) proposed the use of an optimal parameter μ^{opt} in the stabilization matrix. The factor μ^{opt} can be seen as the smallest parameter which yields an hourglass-free deformation pattern and it can be obtained as follows:

$$\mu^{opt} = \mu \frac{H}{E + H}, \tag{36}$$

where E represent the Young's modulus and H is the hardening modulus at the onset of plastification.

Then, by substituting equation 33 in equation 30, the element stabilization stiffness matrix is obtained in the following form:

$$\mathbf{K}^{stab} = \left[\frac{1}{3}\hat{\mathbf{B}}^{t}_{,\xi}(\mathbf{0}) \ \mathbf{E} \ \hat{\mathbf{B}}_{,\xi}(\mathbf{0}) + \frac{1}{3}\hat{\mathbf{B}}^{t}_{,\eta}(\mathbf{0}) \ \mathbf{E} \ \hat{\mathbf{B}}_{,\eta}(\mathbf{0}) + \frac{1}{3}\hat{\mathbf{B}}^{t}_{,\zeta}(\mathbf{0}) \ \mathbf{E} \ \hat{\mathbf{B}}_{,\zeta}(\mathbf{0}) + \frac{1}{9}\hat{\mathbf{B}}^{t}_{,\xi\eta}(\mathbf{0}) \ \mathbf{E} \ \hat{\mathbf{B}}_{,\xi\eta}(\mathbf{0}) + \frac{1}{9}\hat{\mathbf{B}}^{t}_{,\eta\zeta}(\mathbf{0}) \ \mathbf{E} \ \hat{\mathbf{B}}_{,\eta\zeta}(\mathbf{0}) + \frac{1}{9}\hat{\mathbf{B}}^{t}_{,\xi\zeta}(\mathbf{0}) \ \mathbf{E} \ \hat{\mathbf{B}}_{,\xi\zeta}(\mathbf{0}) \right] V_e . \tag{37}$$

The element developed so far is free of volumetric locking and has no spurious singular modes. However, it is not suitable to plate/shell analysis owing to the shear and membrane locking in thin structures and it cannot pass the patch test if the mesh is irregular.

To remove shear locking, it is shown by Hu and Nagy (1997) that the gradient submatrices corresponding to the assumed shear strain is written in an orthogonal corotational coordinate system rotating with the element and each shear-strain component is linearly interpolated in one referential coordinate direction only:

$$\boldsymbol{\varepsilon}_{xy}(\xi,\eta,\zeta) = \boldsymbol{\varepsilon}_{xy}(\mathbf{0}) + \hat{\boldsymbol{\varepsilon}}_{xy,\zeta}(\mathbf{0})\zeta , \tag{38}$$

$$\boldsymbol{\varepsilon}_{yz}(\xi,\eta,\zeta) = \boldsymbol{\varepsilon}_{yz}(\mathbf{0}) + \hat{\boldsymbol{\varepsilon}}_{yz,\xi}(\mathbf{0})\xi , \tag{39}$$

$$\boldsymbol{\varepsilon}_{xz}(\xi,\eta,\zeta) = \boldsymbol{\varepsilon}_{xz}(\mathbf{0}) + \hat{\boldsymbol{\varepsilon}}_{xz,\eta}(\mathbf{0})\eta , \tag{40}$$

which implies:

$$\hat{\mathbf{B}}_{xy,\xi}(\mathbf{0}) = \hat{\mathbf{B}}_{xy,\eta}(\mathbf{0}) = \hat{\mathbf{B}}_{xy,\xi\eta}(\mathbf{0}) = \hat{\mathbf{B}}_{xy,\eta\zeta}(\mathbf{0}) = \hat{\mathbf{B}}_{xy,\xi\zeta}(\mathbf{0}) = \mathbf{0} , \tag{41}$$

$$\hat{\mathbf{B}}_{yz,\eta}(\mathbf{0}) = \hat{\mathbf{B}}_{yz,\zeta}(\mathbf{0}) = \hat{\mathbf{B}}_{yz,\xi\eta}(\mathbf{0}) = \hat{\mathbf{B}}_{yz,\eta\zeta}(\mathbf{0}) = \hat{\mathbf{B}}_{yz,\xi\zeta}(\mathbf{0}) = \mathbf{0} , \tag{42}$$

$$\hat{\mathbf{B}}_{xz,\xi}(\mathbf{0}) = \hat{\mathbf{B}}_{xz,\zeta}(\mathbf{0}) = \hat{\mathbf{B}}_{xz,\xi\eta}(\mathbf{0}) = \hat{\mathbf{B}}_{xz,\eta\zeta}(\mathbf{0}) = \hat{\mathbf{B}}_{xz,\xi\zeta}(\mathbf{0}) = \mathbf{0} , \tag{43}$$

where $\hat{\mathbf{B}}_{xy}$, $\hat{\mathbf{B}}_{yz}$ e $\hat{\mathbf{B}}_{xz}$ are the gradient matrices corresponding to the deviatoric strain components $\hat{\boldsymbol{\varepsilon}}_{xy}$, $\hat{\boldsymbol{\varepsilon}}_{yz}$ e $\hat{\boldsymbol{\varepsilon}}_{xz}$, respectively.

The one-point quadrature element will pass in the patch test when it is skewed if the gradient matrix $\mathbf{B}_a(0)$ is replaced by the uniform gradient $\mathbf{B}'_a(0)$ defined by Flanagan and Belytschko (1983) as:

$$\mathbf{B}'_a = \frac{1}{V_e}\int_{V_e} \mathbf{B}_a(\xi,\eta,\zeta) \ dV . \tag{44}$$

4 CORROTATIONAL APPROACH FOR PHYSICAL AND GEOMETRICALLY NONLINEAR ANALYSIS

It has been shown that the elimination of the shear locking depends on the proper treatment of the shear strain. It is necessary to attach a local coordinate system to the element so that the strain tensor in this local system is relevant for the treatment. The corotational system described in Liu *et al*. (1998) is employed for this purpose. By using the corotational system, the integration of the elasto-plastic constitutive equations becomes easier.

Theoretically, the motion of a continuous medium can always be decomposed into a rigid body motion followed by a pure deformation. If the finite element discretization is fine enough to provide a valid approximation of the continuum, this decomposition can be

performed at the element level. If the rigid body motion is eliminated from the total displacement field which corresponds to large displacements and rotation but small strains, the pure deformation part is always a small quantity relative to the element dimensions.

4.1 Corotational stress updates

For stress and strain updates, we assume that all variables at the previous load step t_n are known. Then, it is only necessary to calculate the strain increment from the displacement field within the load increment $[t_n, t_{n+1}]$, and the procedure described by Liu *et al*. (1998) to calculate the deformation part ($\Delta\hat{\mathbf{u}}^{\text{def}}$) of the displacement increment in a corotational system is used. In this work, $\Delta\hat{\mathbf{u}}^{\text{def}}$ is referred to the mid-point configuration ($t_{n+1/2}$).

Denoting the spatial coordinates of the previous load step configuration, Ω_n, and the current configuration, Ω_{n+1}, as $\boldsymbol{x}_n$ e $\boldsymbol{x}_{n+1}$ in the fixed global Cartesian coordinate system Ox, the coordinates in the corresponding corotational Cartesian coordinate system, $O\hat{x}_n$ and $O\hat{x}_{n+1}$, can be obtained by the following transformation rules:

$$\hat{\mathbf{x}}_n = \mathbf{R}_n \mathbf{x}_n , \tag{45}$$

$$\hat{\mathbf{x}}_{n+1} = \mathbf{R}_{n+1} \mathbf{x}_{n+1} , \tag{46}$$

where $\mathbf{R}_n$ and $\mathbf{R}_{n+1}$ are the orthogonal transformation matrices which rotates the global coordinate system to the corresponding corotational coordinate system, respectively (defined in Liu *et al*. (1998) and in Duarte Filho and Awruch (2004)).

Since the strain increment is referred to the configuration at $t = t_{n+1/2}$, assuming the velocities within the increment $[t_n, t_{n+1}]$ are constant, it is obtained:

$$\mathbf{x}_{n+1/2} = \frac{1}{2}\left(\mathbf{x}_n + \mathbf{x}_{n+1}\right), \tag{47}$$

$$\hat{\mathbf{x}}_{n+1/2} = \mathbf{R}_{n+1/2} \mathbf{x}_{n+1/2} . \tag{48}$$

Similar to polar decomposition, an incremental deformation can be separated into the summation of the pure deformation and the pure rotation. Letting $\Delta\mathbf{u}$ indicate the displacement increment within the load increment $[t_n, t_{n+1}]$, it may be written:

$$\Delta\mathbf{u} = \Delta\mathbf{u}^{\text{def}} + \Delta\mathbf{u}^{\text{rot}} , \tag{49}$$

where $\Delta\mathbf{u}^{\text{def}}$ e $\Delta\mathbf{u}^{\text{rot}}$ are, respectively, the deformation part and the pure rotation part of the displacement increment in the global coordinate system.

In order to obtain the deformation part of the displacement increment referred to the configuration at $t = t_{n+1/2}$, it is necessary to find the rigid rotation from Ω_n to Ω_{n+1}.

It can be shown that the total rotation displacement increment can be expressed as:

$$\Delta\mathbf{u}^{\text{rot}} = \mathbf{x}_{n+1} - \mathbf{x}_n - \mathbf{R}^t_{n+1/2}\left(\hat{\mathbf{x}}_{n+1} - \hat{\mathbf{x}}_n\right) = \Delta\mathbf{u} - \mathbf{R}^t_{n+1/2}\left(\hat{\mathbf{x}}_{n+1} - \hat{\mathbf{x}}_n\right). \tag{50}$$

Then, the deformation part of the displacement increment referred to $\Omega_{n+1/2}$ is:

$$\Delta\mathbf{u}^{\text{def}} = \Delta\mathbf{u} - \Delta\mathbf{u}^{\text{rot}} = \mathbf{R}^t_{n+1/2}\left(\hat{\mathbf{x}}_{n+1} - \hat{\mathbf{x}}_n\right). \tag{51}$$

Therefore, the deformation displacement increment in the corotational system $O\hat{x}_{n+1/2}$ is obtained as:

$$\Delta\hat{\mathbf{u}}^{\text{def}} = \mathbf{R}_{n+1/2}\Delta\mathbf{u}^{\text{def}} = \hat{\mathbf{x}}_{n+1} - \hat{\mathbf{x}}_n \,. \tag{52}$$

Since the corotational coordinate system rotates with the configuration, it is used the corotational Cauchy stress, which is objective, as stress measure. The rate of deformation (or velocity strain vector), $\dot{\boldsymbol{\varepsilon}}$, also defined in the corotational coordinate system, is used as the measure of the strain rate:

$$\dot{\boldsymbol{\varepsilon}} = \hat{\mathbf{d}} = \frac{1}{2}\left[\frac{\partial\hat{\mathbf{v}}^{\text{def}}}{\partial\hat{\mathbf{x}}} + \left(\frac{\partial\hat{\mathbf{v}}^{\text{def}}}{\partial\hat{\mathbf{x}}}\right)^t\right], \tag{53}$$

where $\hat{\mathbf{v}}^{\text{def}}$ is the deformation part of the velocity in the corotational system $\hat{\mathbf{x}}$.

Then, the strain increment is given by the mid-point integration of the velocity strain tensor,

$$\Delta\hat{\boldsymbol{\varepsilon}} = \int_{t_n}^{t_{n+1}} \hat{\mathbf{d}} \;\; \mathrm{d}\tau \doteq \frac{1}{2}\left[\frac{\partial\ \Delta\hat{\mathbf{u}}^{\text{def}}}{\partial\ \hat{\mathbf{x}}_{n+1/2}} + \left(\frac{\partial\ \Delta\hat{\mathbf{u}}^{\text{def}}}{\partial\ \hat{\mathbf{x}}_{n+1/2}}\right)^t\right]. \tag{54}$$

Once the strain increment is obtained by equation 54, the stress increment can be calculated with the elasto-plastic scheme described in Section 5, and the total strain and stress can then be updated as:

$$\hat{\boldsymbol{\varepsilon}}_{n+1} = \hat{\boldsymbol{\varepsilon}}_n + \Delta\hat{\boldsymbol{\varepsilon}} \,, \tag{55}$$

$$\hat{\boldsymbol{\sigma}}_{n+1} = \hat{\boldsymbol{\sigma}}_n + \Delta\hat{\boldsymbol{\sigma}} \,. \tag{56}$$

4.2 Constitutive equations and solution of the incremental system of equations

As the material rate for the Cauchy stress tensor is not a frame-invariant rate, it is employed the Green-Naghdi objective rate, which, according to Liu *et al.* (1998) and Duarte Filho and Awruch (2004), gives the following material tangent matrix:

$$\mathbf{T}(\boldsymbol{\sigma}) = \begin{bmatrix} \mathbf{C}_{6x6} & \mathbf{0}_{6x3} \\ \mathbf{0}_{3x6} & \mathbf{0}_{3x3} \end{bmatrix} + \hat{\mathbf{T}}(\boldsymbol{\sigma}), \tag{57}$$

where $\mathbf{0}_{m\times n}$ denotes the $m\times n$ zero matrix, $\mathbf{C}$ is a 6×6 stress-strain matrix and $\hat{\mathbf{T}}(\boldsymbol{\sigma})$, the initial-stress matrix, is defined below:

$$\hat{\mathbf{T}}(\boldsymbol{\sigma}) = \begin{bmatrix}
2\sigma_{11} & 0 & 0 & \sigma_{12} & 0 & \sigma_{13} & \sigma_{12} & 0 & -\sigma_{13} \\
 & 2\sigma_{22} & 0 & \sigma_{12} & \sigma_{23} & 0 & -\sigma_{12} & \sigma_{23} & 0 \\
 & & 2\sigma_{33} & 0 & \sigma_{23} & \sigma_{13} & 0 & -\sigma_{23} & \sigma_{13} \\
 & & & \frac{\sigma_{11}+\sigma_{22}}{2} & \frac{\sigma_{13}}{2} & \frac{\sigma_{23}}{2} & \frac{\sigma_{22}-\sigma_{11}}{2} & \frac{\sigma_{13}}{2} & -\frac{\sigma_{23}}{2} \\
 & & & & \frac{\sigma_{22}+\sigma_{33}}{2} & \frac{\sigma_{12}}{2} & -\frac{\sigma_{13}}{2} & \frac{\sigma_{33}-\sigma_{22}}{2} & \frac{\sigma_{12}}{2} \\
 & & & & & \frac{\sigma_{33}+\sigma_{11}}{2} & \frac{\sigma_{23}}{2} & -\frac{\sigma_{12}}{2} & \frac{\sigma_{11}-\sigma_{33}}{2} \\
 & & \text{symm.} & & & & \frac{\sigma_{11}+\sigma_{22}}{2} & -\frac{\sigma_{13}}{2} & -\frac{\sigma_{23}}{2} \\
 & & & & & & & \frac{\sigma_{22}+\sigma_{33}}{2} & -\frac{\sigma_{12}}{2} \\
 & & & & & & & & \frac{\sigma_{33}+\sigma_{11}}{2}
\end{bmatrix} \tag{58}$$

The $\mathbf{T}(\boldsymbol{\sigma})$ matrix is arranged to be compatible with the following ordering of strain and rotation components:

$$\boldsymbol{\varepsilon}^t = \left[\dot{\varepsilon}_{11}\ \dot{\varepsilon}_{22}\ \dot{\varepsilon}_{33}\ \dot{\varepsilon}_{12}\ \dot{\varepsilon}_{23}\ \dot{\varepsilon}_{31}\ \dot{\omega}_{12}\ \dot{\omega}_{23}\ \dot{\omega}_{31}\right]. \tag{59}$$

Then, the equilibrium equation at the j^{th} iteration can be written in the corotational coordinate system as:

$$\hat{\mathbf{K}}_{j-1}\,\Delta\hat{\mathbf{U}} = \hat{\mathbf{P}}_j - \hat{\mathbf{f}}_{j-1}, \tag{60}$$

where $\Delta\hat{\mathbf{U}}$ is the displacement increment vector; $\hat{\mathbf{P}}_j$ is the externally applied nodal point forces and the tangent stiffness matrix $\hat{\mathbf{K}}_{j-1}$ and the internal nodal force vector $\hat{\mathbf{f}}_{j-1}$ are:

$$\hat{\mathbf{K}}_{j-1} = \mathbf{B}''^t(\mathbf{0})\left(\mathbf{C} + \hat{\mathbf{T}}_{j-1}\right)\mathbf{B}'(\mathbf{0}) + \mathbf{K}^{stab}, \tag{61}$$

$$\hat{\mathbf{f}}_{j-1} = \mathbf{f}^e + \mathbf{f}^{hg}. \tag{62}$$

The tangent stiffness and nodal forces are transformed into the global coordinate system as:

$$\mathbf{K}_j = \mathbf{R}_j^t \hat{\mathbf{K}}_j \mathbf{R}_j, \tag{63}$$

$$\mathbf{r}_j = \mathbf{R}_j^t\left(\hat{\mathbf{P}}_j - \hat{\mathbf{f}}_{j-1}\right) = \mathbf{R}_j^t\ \ \hat{\mathbf{r}}_j, \tag{64}$$

where $\mathbf{R}$ is the transformation matrix of the corotational system defined by Liu *et al*. (1998) and by Duarte Filho and Awruch (2004).

5 ELASTO-PLASTIC CONSTITUTIVE EQUATION

During a typical step of an elasto-plastic finite element analysis, the forces are applied in increments and the corresponding nodal displacement increments are found from the global equilibrium equations. Once these displacements are known, the strain increments at the integration points within each element are determined using the strain displacement relations. If the stresses associated with an imposed strain increment cause plastic yielding, the elasto-plastic constitutive equation may be written in the following incremental form:

$$\Delta\boldsymbol{\sigma} = \mathbf{C}_{ep}\Delta\boldsymbol{\varepsilon}. \tag{65}$$

According to Owen and Hinton (1980), the elasto-plastic stress-strain matrix, $\mathbf{C}_{ep}$, for the particular case of an associated flow rule is given by:

$$\mathbf{C}_{ep} = \mathbf{C}_e - \frac{\mathbf{C}_e\mathbf{a}\mathbf{a}^t\mathbf{C}_e}{H + \mathbf{a}^t\mathbf{C}_e\mathbf{a}}, \tag{66}$$

where $\mathbf{C}_e$ is the elastic stress-strain matrix, $\mathbf{a}$ is the yield surface gradient and H is the hardening modulus, that can be expressed, in the case of linear hardening, as a function of the elastic modulus E and the plastic tangent modulus E_T as:

$$H = \frac{E_T}{1 - E_T/E}. \tag{67}$$

5.1 Integration of the constitutive equations

According to Liu *et al.* (1998), with the use of a corotational system, the integration of the finite deformation elasto-plastic constitutive equations takes a simple form, as the small deformation theory. The integration of the constitutive equations is performed at element level in the corotational system. The integration scheme, proposed by Sloan *et al.* (2001) is used in this work to deal with the physical nonlinearity. The integration scheme can be summarized in computing an elastic trial stress state, finding the yield surface intersection point (considering also the case of elasto-plastic unloading), updating the stresses and restoring the stresses to the yield surface.

With $\boldsymbol{\sigma}_0$ denoting the initial stress state, the elastic trial stress state can be easily computed according to $\boldsymbol{\sigma}_e = \boldsymbol{\sigma}_0 + \Delta\boldsymbol{\sigma}_e$, where $\Delta\boldsymbol{\sigma}_e = \mathbf{C}_e \Delta\boldsymbol{\varepsilon}$. The problem of finding the stresses at the yield surface intersection point $\boldsymbol{\sigma}_{int}$ is equivalent to finding the scalar quantity α which satisfies the following non-linear equation:

$$f(\boldsymbol{\sigma}_0 + \alpha \mathbf{C}_e \Delta\boldsymbol{\varepsilon}) = f(\boldsymbol{\sigma}_{int}) = 0, \tag{68}$$

where f is the yield function. A value of $\alpha = 0$ indicates that $\Delta\boldsymbol{\varepsilon}$ causes purely plastic deformation, while a value of $\alpha = 1$ indicates purely "elastic" deformation. Thus, for an elastic to plastic transition, we have $0 < \alpha < 1$ and the "elastic" part of the stress increment is given by $\alpha \mathbf{C}_e \Delta\boldsymbol{\varepsilon}$. If the initial stress state is lying on the yield surface and the angle θ between the yield surface gradient $\mathbf{a}_0$ and the tangential elastic stress increment $\Delta\boldsymbol{\sigma}_e$ is larger than 90º, the stress increment may cross the yield surface twice. This possibility is caused by the use of a tolerance to the value of the yield function which permits the stresses to lye just outside the yield surface, and it can be checked with:

$$\cos\theta = \frac{\mathbf{a}_0^t \Delta\boldsymbol{\sigma}_e}{\|\mathbf{a}_0\|_2 \, \|\Delta\boldsymbol{\sigma}_e\|_2}, \tag{69}$$

where $\| \, . \, \|_2$ is the norm in the space L_2. Sloan *et al.* (2001) gives a detailed algorithmic description of the method to find α, with sufficient details in order to be implemented in a finite element code.

Once α is found, the portion of the tangential elastic stress increment $\Delta\boldsymbol{\sigma}_e$ that corresponds to plastic deformation is computed with $(1-\alpha)\Delta\boldsymbol{\sigma}_e$ and used to compute the stress increment:

$$\Delta\boldsymbol{\sigma} = \Delta\boldsymbol{\sigma}_e - \Delta\lambda \mathbf{C}_e \mathbf{a}, \tag{70}$$

where the plastic strain-rate multiplier, $\Delta\lambda$, which for the particular case of the von Mises yield criterion with isotropic hardening is equal to the equivalent plastic strain, can be found as follows:

$$\Delta\lambda = \frac{\mathbf{a}^t \Delta\boldsymbol{\sigma}_e}{H + \mathbf{a}^t \mathbf{C}_e \mathbf{a}}. \tag{71}$$

5.2 Correction of stresses to the yield surface

At the end of each increment in the explicit integration process, the stresses may diverge from the yield condition. The extent of this violation, which is commonly known as yield surface "drift", depends on the accuracy of the integration scheme and the nonlinearity of the

constitutive relations. Sloan (1987) suggested that, once the integration is performed accurately, the amount of yield surface drift will be small and any remedial action is optional. Other authors, including Crisfield (1991), strongly advocate some form of iterative stress correction as the effects of violating the yield condition are cumulative.

The radial return algorithm, used to correct the stresses in this work, consists in finding the closest-point-projection of the stress state onto the yield surface, if the stress state lies outside the yield surface. A small correction to the plastic strain-rate multiplier is computed with the following equation:

$$\delta\lambda = \frac{f_0}{H + \mathbf{a}^t \mathbf{C}_e \mathbf{a}}, \tag{72}$$

where f_0 is the value of the yield function for the uncorrected stresses. The stresses and the equivalent plastic strain are then updated according to the following expressions:

$$\boldsymbol{\sigma} = \boldsymbol{\sigma}_0 - \delta\lambda \mathbf{C}_e \mathbf{a}, \tag{73}$$

$$\bar{\varepsilon}^{\mathrm{pl}} = \bar{\varepsilon}^{\mathrm{pl}}_{\mathbf{0}} - \delta\lambda, \tag{74}$$

where the subscript *0* in equation 73 and equation 74, as well as in equation 69 refers to uncorrected variables.

6 NUMERICAL EXAMPLES

Numerical applications involving the von Mises as well as the Mohr-Coulomb yield criterion exhibiting highly nonlinear behavior, are presented to test and to verify the element performance for physical and nonlinear geometrically analysis. Results are compared with those reported by other authors and with the commercial code ABAQUS (2004).

6.1 Elastic-plastic cantilever beam

This simulation presents the elasto-plastic response of a cantilever beam subjected to a transverse shear load of 80 kN at one end. The three displacements degrees of freedom of all the nodes at the fixed end are prescribed. The length of the beam is L = 24.0 m, while the width is B = 1.0 m and the height is H = 4.0 m. The material has isotropic hardening with bilinear uniaxial stress-strain relation and the material parameters are: elastic modulus E = 1.0 × 10^4 kN/m^2, Poisson's ratio ν = 0.3, initial yield stress σ_0 = 3.0 × 10^2 kN/m^2, and the tangential modulus after yielding, E_T = 1.0 × 10^3 kN/m^2. An schematic representation of the example can be found on Figure 1.

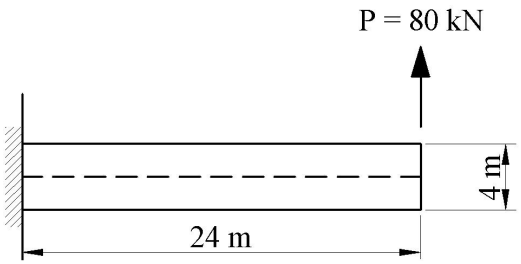

Figure 1: Elastic-plastic cantilever beam

The results achieved with the present element are compared with those given by the 8 node brick element with incompatible mode (called C3D8I) in ABAQUS. The mesh used in the calculations with the present element and C3D8I has 48×8×1 (length×height×width)

elements. The initial geometry configuration and the final deformed mesh can be seen in Figure 2.

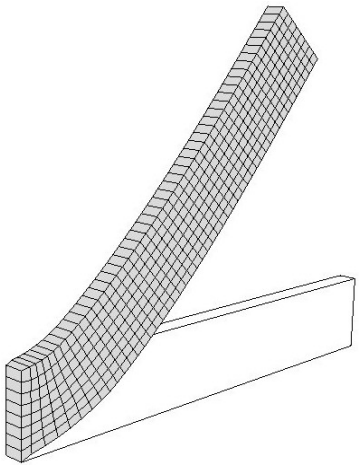

Figure 2: Initial geometry and deformed mesh

The deflection on the mid-surface is shown in Figure 3. It may be observed that the result is very close to those given by the C3D8I element of ABAQUS.

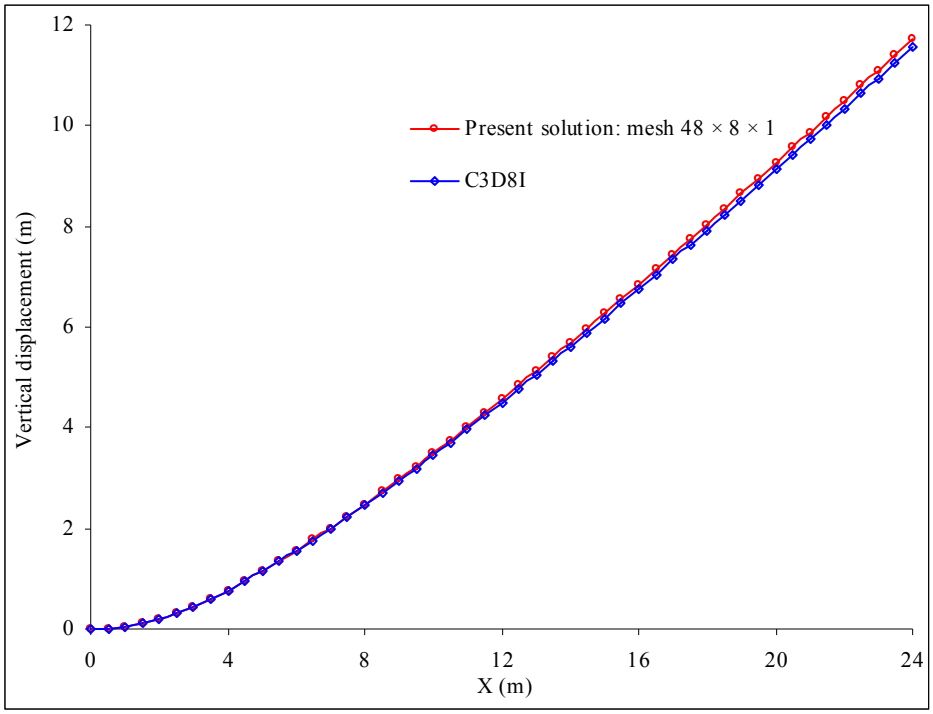

Figure 3: Deflection on the mid-surface of elastic-plastic beam

6.2 Square plate under concentrated load

A concentrated load of 70 kN is applied at the center of a square plate with length $L = 40$ m and thickness $t = 0.4$ m, as shown on Figure 4. The material is an elastic-plastic model with isotropic hardening and Young's modulus $E = 3.0 \times 10^7$ kN/m^2, tangential modulus after yielding, $E_T = 3.0 \times 10^6$ kN/m^2, Poisson's ratio $\nu = 0.3$ and initial yield stress $\sigma_0 = 4.0 \times 10^4$ kN/m^2. The plate has simply supported edges and due to symmetry, only a quarter of the plate

is modeled with 24×24×6 three-dimensional elements (6 elements were used in the thickness direction).

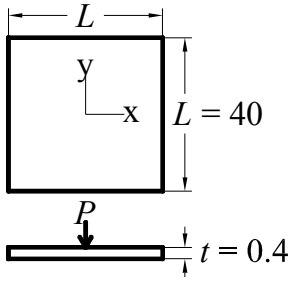

Figure 4: Square plate under concentrated load

The present solution is compared with results obtained by the element C3D8I, in ABAQUS. The plots of central deflection vs concentrated load is given in Figure 5.

Analyzing the results it is possible to see that the present solution agrees very well with the solution achieved with ABAQUS.

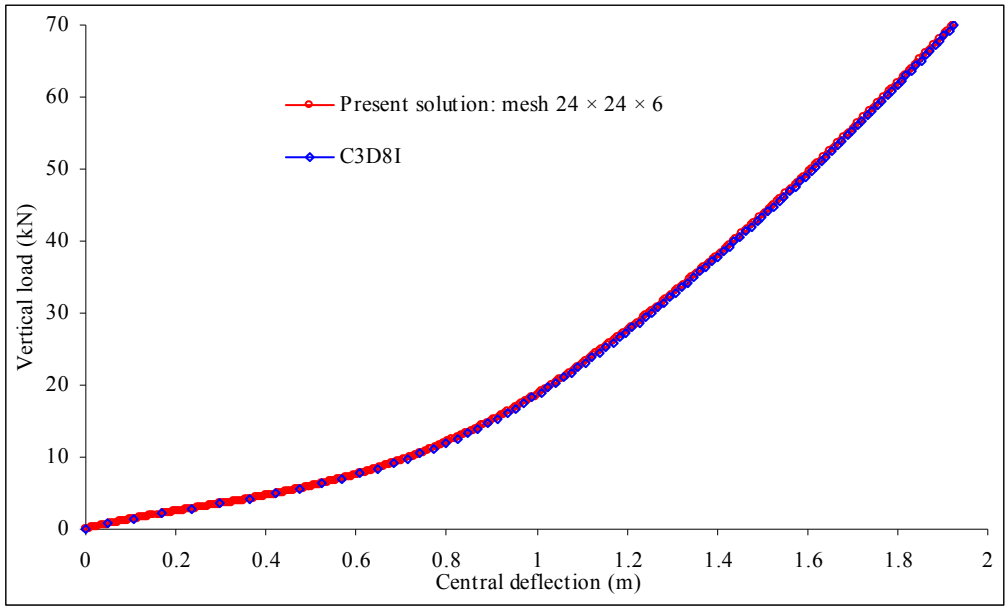

Figure 5: Vertical load *vs* central deflection

6.3 Mohr-Coulomb slope stability analysis

A slope stability analysis with the Mohr-Coulomb yield criterion is performed in this example. The slope geometry and boundary conditions are presented in Figure 6.

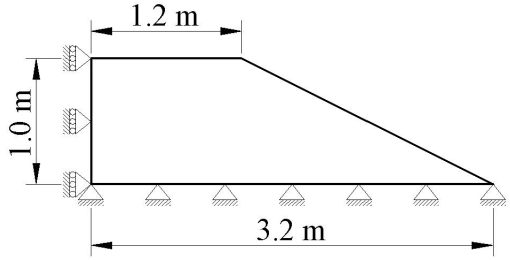

Figure 6: Slope geometry and boundary conditions

The unit weight of the material is $\gamma = 20.0$ kN/m^3, the cohesion $c = 1.0$ kN/m^2, the friction angle $\phi = 40^o$ and the dilatational angle ψ is equal to zero. The material has the Young's modulus $E = 10.5 \times 10^3$ kN/m^2 and the Poisson's ratio $\nu = 0.3$. The out-of-plane displacement degree of freedom is prescribed in all nodes allowing only displacements in the plane. The slope is discretized with a mesh containing 10×10×1 elements (1 element was used in the length direction).

In order to find the factor of safety of the slope, the analysis is performed for several trial factors of safety of the soil parameters ranging form 1.00 to 2.65 and the maximum displacement *vs* factor of safety of each analysis is plotted in Figure 7. The plotted results indicate that the factor of safety of the slope lies around 2.6. It can be seen that the results obtained with the use of the current formulation are close to those achieved by Smith and Griffiths (1997). Bishop and Morgenstern (1960) produced charts for slope stability analysis using slip circle techniques, and these give a factor of safety of 2.505 for the slope considered on this example.

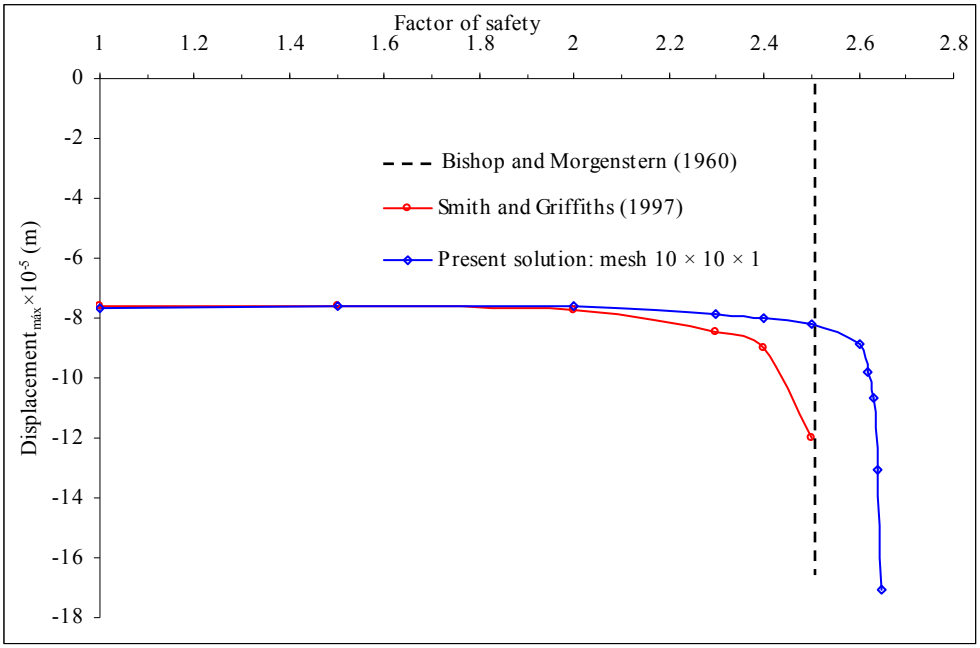

Figure 7: Maximum displacement *vs* factor of safety

The normalized displacements are plotted in Figure 8. The deformed mesh and the nature of the failure mechanism of the slope are also indicated on Figure 8.

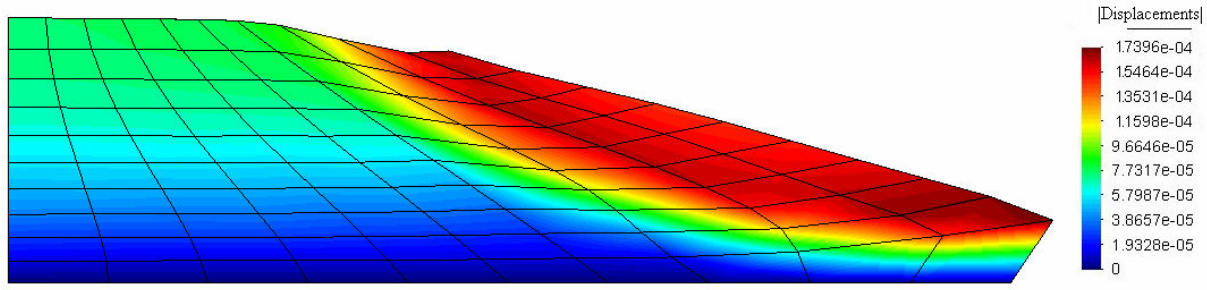

Figure 8: Normalized displacements

6.4 Cylindrical shell with free edges

A cylindrical shell is submitted to a pair of concentrated forces, inducing large displacements and rotations. The geometry of the cylinder is characterized by a length L = 10.35 m, radius R = 4.953 m and a constant thickness t = 0.094 m. The material has isotropic hardening and its properties are: Young's modulus $E = 10.5 \times 10^3$ kN/m^2, Poisson's ratio ν = 0.3125, initial yield stress $\sigma_0 = 1.05 \times 10^2$ kN/m^2, and plastic tangent modulus $E_T = 10.5 \times 10^2$ kN/m^2. No boundary conditions are applied to the free edges of the shell, being the load pair responsible for the equilibrium of the cylinder. Due to symmetry reasons, only one eighth of the cylinder is discretized with a mesh containing 16×8×6 elements (circumference× length×thickness). A schematic representation of the example is presented in Figure 9.

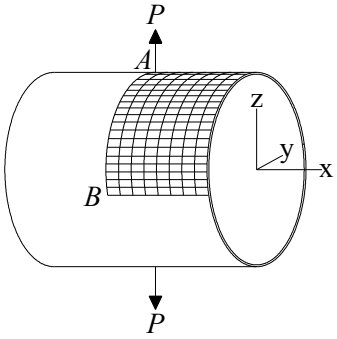

Figure 9: Stretching of a cylinder

In order to obtain the post-buckling response, the Generalized Displacement Control Method, proposed by Yang and Shieh (1990) was implemented. The solution obtained for the displacements with the present element, in both points A and B, *vs* the applied load are compared with the results given by Masud and Tham (2000) and Valente *et al.* (2004). The final deformed configuration is plotted in Figure 10.

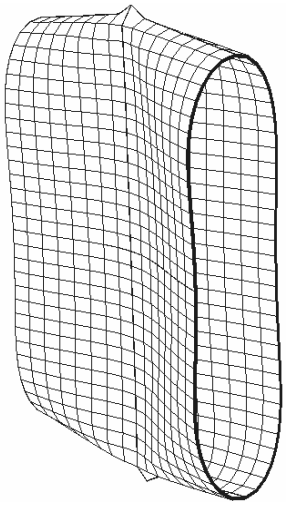

Figure 10: Deformed mesh due to the 40 kN load

In Figure 11 results obtained with the use of the current formulation compared with those published in the literature. The present solution agree very well with the results obtained by Valente *et al.* (2004) and is very close to the solution published by Masud and Tham (2000).

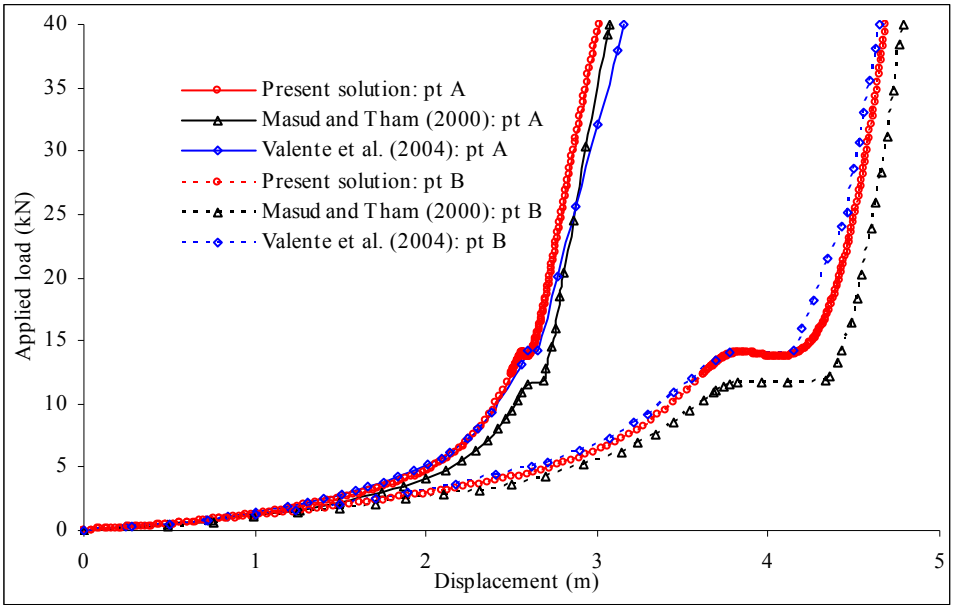

Figure 11: Applied load *vs* displacement

7 CONCLUSIONS

An isoparametric hexahedrical finite element with eight nodes and one-point quadrature was formulated and it was applied to analyze physical and geometrically nonlinear problems involving plates and shells. The Mohr-Coulomb as well as the Von Mises yield criterion with isotropic hardening, in the context of structures with finite displacements and rotations, was used. A corotational formulation was employed to deal with the geometrical nonlinear analysis while an explicit algorithm was implemented for the elasto-plastic analysis. Good results were obtained when compared to those presented by other authors and those obtained using a commercial software, and no volumetric and/or shear locking were detected in any case.

Future works will extend applications of this element to geotechnical problems, using more complex constitutive equations, and kinematic, as well as mixed hardening, will be implemented.

REFERENCES

A. Masud and C. L. Tham. Three-dimensional corotational framework for elasto-plastic analysis of multilayered composite shells. *AIAA Journal*, 38:2320-2327, 2000.

A. W. Bishop and N. Morgenstern. Stability coefficients for earth slopes. *Géotechnique*, 10:129-150, 1960.

ABAQUS v 6.5-1. *ABAQUS Analysis User's Manual.* ABAQUS, Inc, 2004

D. P. Flanagan and T. Belytschko. A uniform strain hexahedron and quadrilateral with orthogonal hourglass control. *International Journal for Numerical Methods in Engineering,* 17:679-706, 1983.

D. R. J. Owen and E. Hinton. *Finite Elements in Plasticity: Theory and Practice*. Pineridge Press Limited, 1980.

I. M. Smith and D. V. Griffiths. *Programming the finite element method.* John Wiley & Sons, 1997

L. A. Duarte Filho and A. M. Awruch. Geometrically nonlinear static and dynamic analysis of shells and plates using the eight-node hexahedral element with one-point quadrature. *Finite Elements in Analysis and Design*, 40:1297-1315, 2004.

M.A. Crisfield, 1991. *Non-linear Finite Element Analysis of Solids and Structures*, volume 1. John Wiley & Sons, 1991.

R. A. F. Valente, R. J. A. Souza and R. M. N. Jorge. An enhanced strain 3D element for large deformation elastoplastic thin-shell applications. *Computational Mechanics,* 34:38-52, 2000.

S. Reese. On a physically stabilized one point finite element formulation for three-dimensional finite elasto-plasticity. *Computer Methods in Applied Mechanics and Engineering,* 194:4685-4715, 2005.

S. W. Sloan, A. J. Abbo, and D. Sheng. Refined explicit integration of elastoplastic models with automatic error control. *Engineering Computations,* 18:121-154, 2001.

S. W. Sloan. Substepping schemes for the numerical integration of elastoplastic stress-strain relations. *International Journal for Numerical Methods in Engineering*, 24:893-911, 1987.

Y.-B. Yang and M. S. Shieh. Solution method for nonlinear problems with multiple critical points. *AIAA Journal*, 28:2110-2116, 1990.

Y.-K. Hu and L. I. Nagy. A one-point quadrature eight-node brick element with hourglass control. *Computers & Structures*, 65:893-902, 1997.

W. K. Liu, Y. Guo, S. Tang and T. Belytschko. A multiple quadrature eight-node hexahedral finite element for large deformation elastoplastic analysis. *Computer Methods in Applied Mechanics and Engineering,* 154:69-132, 1998.

W. K. Liu, Y. -K. Hu, and T. Belytschko. Multiple quadrature underintegrated finite elements. *International Journal for Numerical Methods in Engineering,* 37:3263-3289, 1994.